# Modeling of Surface Mechanical Behaviors of Soft Elastic Solids: Theory and Examples

| | |
|---|---|
| Journal: | *Soft Matter* |
| Manuscript ID | SM-ART-03-2020-000556.R1 |
| Article Type: | Paper |
| Date Submitted by the Author: | 23-Jun-2020 |
| Complete List of Authors: | Liu, Zezhou; Cornell University, Department of Mechanical and Aerospace Engineering<br>Jagota, Anand; Lehigh University, Bioengineering<br>Hui, Chung-Yuen; Cornell University, Theoretical and Applied Mechanics |
| | |

SCHOLARONE™
Manuscripts

# Modeling of Surface Mechanical Behaviors of Soft Elastic Solids: Theory and Examples

Zezhou Liu[1], Anand Jagota[2] and Chung-Yuen Hui[1,*]

[1]Department of Mechanical and Aerospace Engineering, Field of Theoretical and Applied Mechanics, Cornell University, Ithaca, NY 14853, USA

[2]Departments of Bioengineering and of Chemical & Biomolecular Engineering, 111 Research Drive, Lehigh University, Bethlehem, PA 18015, USA

*Correspondence to: 322 Kimball Hall, Cornell University, Ithaca, NY 14853, USA

E-mail address: ch45@cornell.edu (C.-Y. Hui)

**Abstract:** Surfaces of soft solids can have significant surface stress, extensional modulus and bending stiffness. Previous theoretical studies have usually examined cases in which both the surface stress and bending stiffness are constant, assuming small deformation. In this work we consider a general formulation in which the surface can support large deformation and carry both surface stresses and surface bending moments. We demonstrate that the large deformation theory can be reduced to the classical linear theory (Shuttleworth Equation). We obtain exact solutions for problems of an inflated cylindrical shell and bending of a plate with a finite thickness. Our analysis illustrates the different manners in which surface stiffening and surface bending stabilize these structures. We discuss how the complex surface constitutive behaviors affect the stress field of the bulk. Our calculation provides insights into effects of strain-dependent surface stress and surface bending in the large deformation regime, and can be used as a model to implement surface finite elements to study large deformation of complex structures.

**Keywords:** large deformation; surface bending moment; strain-dependent surface stress.

## 1. Introduction

Molecular structures of materials near the surfaces are exposed to a local environment distinctly different from those inside the bulk, and this difference gives rise to the surface energy (a scalar) and surface stress (a 2D tensor) in liquids and in solids.[1–3] For example, in simple liquids, the surface region of a few nanometers typically has a lower density and carries a net tensile surface stress. This stress tends to shrink the surface area

reducing the surface-to-volume ratio. Because of the molecular mobility in liquids, the interior molecules can move freely and quickly to the surface during deformation, and this results in an isotropic, strain-independent surface stress at the macroscopic length and time scales. By contrast, the molecular mobility in solids is limited; as a result, solids can have much more complex surface mechanical properties. In most situations, the effects of surface stress are felt over a characteristic length scale, the elasto-capillary length, defined as $\sigma/E$, where $\sigma$ is the magnitude of the surface stress and $E$ is the Young's modulus of the solid.[4,5] For conventional stiff materials, e.g. metals and ceramics, the value of elasto-capillary length is extremely small, on the order of angstroms.[4] Thus, the effect of surface stress is insignificant and negligible for these stiff materials. However, over the past decade, many studies have established the important and often dominant role of the surface of *soft* solids, such as gels and biomaterials, in their mechanical responses. For instance, surface stress can flatten sharp features by smoothing corners and undulations[6–8]; drive instabilities[9]; stiffen fluid-solid composites[10]; significantly affect the opening of cracks in a soft material[11–13]; invalidate the classical contact and adhesive mechanism by the Hertz and Johnson-Kendall-Roberts (JKR) theories[14–19]; violate the classical Young Equation[4,8,20–30]; and inhibit the flow field in porous media.[31]

The majority of these recent investigations on the role of surfaces in surface mechanical phenomena for soft solids consider the surface to possess a constant and isotropic surface stress, and much less attention has been paid to more complex surface properties such as surface elasticity (strain-dependent resistance to stretching) and surface bending (resistance to surface curvature change). This is natural since typically many soft solids – such as gels, elastomers, and most biomaterials – either contain a significant solvent component or have molecular structures that comprise chain-like molecules that locally are fluid-like. This leads to the expectation that the surface stress in such soft solids is isotropic and constant. However, recent experiments[32,33] have shown that surfaces of certain polymers can have extensional surface elasticity. Interestingly, there is little work on how the surfaces of soft solids respond to surface bending moments even though biophysicists and mechanicians have studied surfaces such as lipid bilayers and vesicles where resistance to stretching is high, deformations generally conserve area, and the surface strain energy density is dominated by bending.[34,35] For example, Kusumaatmaja et al.[36] have shown that the mechanics of the contact line between lipid bilayer membranes is governed by both surface bending and stress. A different example of surface bending is where a new hard phase separates a soft solid from the air – e.g., a thin silica film that forms on the surface of an elastomer (e.g., polydimethylsiloxane) exposed to ultraviolet ozonolysis (UVO) or oxygen plasma.[37,38] Lapinski et al.[39] recently demonstrated that, after UVO treatment, the surface of a commonly used PDMS has significant surface stress ($\sigma_0 \sim 2.5$ N/m), and strong extensional elasticity ($B \sim 21$ N/m). In addition, experimental profiles could be matched by results of finite element analysis only when the surface also resisted bending, with bending stiffness of ($k_b \sim 1.6 \times 10^{-13}$ Nm). In general, surface bending would be important at a

characteristic length scale of $\left(k_b / E\right)^{1/3} \sim 375$ nm in this case. We note that theories that include couple stresses and micro-rotations have been developed some time ago both for bulk[40,41] and surface behavior[42–45], and we will build upon the latter.

Motivated by these examples, recent theoretical studies have explored how an elastic substrate with surface stress and bending stiffness responds to a line load by providing a closed form solution of stress and displacement fields near the line load.[46,47] They find that surface bending further regularizes the concentrated elastic fields – the stress and strain field right underneath the line load become continuous. In these works, the basic assumptions were: (1) small deformation based on the linearized theory of elasticity, (2) the surface stress is a constant in-plane and the surface bending moment is proportional to the in-plane curvature. The small strain assumption allows the linearization of curvature as the second derivative of the displacement fields. As a result, the mechanical responses of surface stress, surface bending and bulk can be decoupled and superimposed. Of course, these solutions will break down when the deformation is large as is often the case in soft solids. The effect of large deformations can imply qualitative differences in interpretation. For example, several authors[48–51] have conducted large-deformation analyses of elasto-wetting. Others have studied rounding and flattening of patterned soft solids including effects of large deformation[6,7]. Thus, there is need for a general large deformation formulation coupled with strain-dependent surface stress and surface bending. Here, we focus on studying a class of large deformation surface models. Unlike the linearized version, the surface and bulk responses are nonlinear and cannot be decoupled. Our result contributes to the limited library of analytical solutions for large deformations of soft materials including strain-dependent surface stress and surface bending moment. To illustrate the theory, we give two examples with direct connections to the mechanical behavior of soft materials. The first is a small cavity inflated by internal pressure. This example is motivated by recent interest in cavitation rheology to measure mechanical property of soft materials such as living tissues[52]. In this technique, a cavity is inflated by injecting fluid (water or air) through a needle embedded in the solid. The experiments indicate that surface stress plays an important role in cavity growth. Our second example is motivated by the experiments of Mora et al.,[7] who demonstrated that surface stresses can significantly affect the deformation of slender objects such as beams.

The outline of the paper is as follows. In section 2, we summarize the general theory of elastic surface-substrate interactions which incorporates the effect of elastic resistance to strain and flexural resistance of an effectively elastic sheet attached to the bounding surfaces of solids. In section 3, we study the problem of inflation of a hollow cylindrical cavity in a solid with a surface that can carry strain-dependent surface stresses and surface bending moments. In section 4 we solve a plate bending problem with the same surface constitutive model. These solutions are in closed form. Section 5 concludes with a short summary.

## 2. A general theory of surface-substrate interactions

In this section, we review and summarize a general theory of surface-substrate interactions in which the surface can resist an arbitrary amount of bending, stretching and shearing. For details, the readers are referred to Steigmann and Ogden,[42] Gao et al.,[43] Gurtin and Murdoch,[44] and Green.[45] We demonstrate that the large deformation theory can be reduced to the classical linear theory (Shuttleworth Equation[53]) within the small strain regime. We then specialize this formulation to study 2D plane strain large deformation problems.

### 2.1 Kinematics of finite surface deformation

Consider an elastic solid occupying a region $\Omega_0 \subset \mathbb{R}^3$ with a surface $\partial\Omega_0$ in the reference configuration. A material point in the bulk of the elastic body is identified by its position vector $\mathbf{X}$ with respect to a fixed original point $O$. Assume that the deformation of the solid is defined by a continuously differentiable and invertible map $\chi$. After deformation, the solid occupies a region $\Omega$ that has a surface denoted by $\partial\Omega$, and the material point $\mathbf{X}$ moves to a new position $\mathbf{x}$ under the deformation

$$\mathbf{x} = \chi(\mathbf{X}), \quad \mathbf{X} \in \Omega_0. \tag{1}$$

The bulk deformation gradient tensor $\mathbf{F}$ is defined by

$$\mathbf{F} = \nabla\chi = F_{ij}\mathbf{e}_i \otimes \mathbf{e}_j, \quad F_{ij} = \frac{\partial x_i}{\partial X_j}, \quad i, j \in \{1, 2, 3\}, \tag{2}$$

where $\otimes$ is the standard tensor product, $\{\mathbf{e}_1, \mathbf{e}_2, \mathbf{e}_3\}$ is a fixed orthonormal basis for $\mathbb{R}^3$, and $x_i$, $X_i$ are the Cartesian coordinates of the material point in its reference and current configuration, respectively.
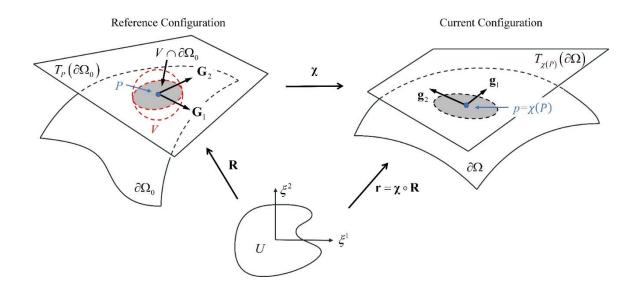
Fig. 1. A regular surface in the reference (before deformation) and current configurations (after deformation).

Consider a coordinate neighborhood of a point $P \in \partial\Omega_0$ in the reference configuration, which is defined as the intersection of the neighborhood $V \subset \mathbb{R}^3$ of $P$ (indicated by the red ball in Fig. 1) and surface $\partial\Omega_0$, i.e., $V \cap \partial\Omega_0$ (indicated by the shaded region in Fig. 1). Assume $\partial\Omega_0$ is a regular surface,[54] thus the coordinate neighborhood can be locally parametrized by curvilinear coordinates $\xi^\alpha$ ($\alpha \in \{1, 2\}$). Here $(\xi^1, \xi^2) \in U$ where $U$ is an open set in $\mathbb{R}^2$. We assume no decohesion, so the deformation of the surface is consistent with that of the bulk solid. This implies that the material point's position satisfies

$$\mathbf{r}(\xi^1, \xi^2) = \chi(\mathbf{R}(\xi^1, \xi^2)), \quad \text{where } \mathbf{R}(\xi^1, \xi^2) \equiv (X_1(\xi^1, \xi^2), X_2(\xi^1, \xi^2), X_3(\xi^1, \xi^2)). \tag{3a,b}$$

Using this parametrization, we introduce the local basis for the tangent planes in the reference and current configurations by

$$\mathbf{G}_\alpha = \mathbf{R}_{,\alpha} \in T_P, \quad \mathbf{g}_\alpha = \mathbf{r}_{,\alpha} \in T_p, \tag{4a,b}$$

respectively, where $T_P$ and $T_p$ are the tangent planes to the surfaces at point $P$ and $p \equiv \chi(P)$, respectively; $(\ )_{,\alpha}$ denotes the usual partial derivative with respect to $\xi^\alpha$, i.e., $(\ )_{,\alpha} = \dfrac{\partial(\ )}{\partial \xi^\alpha}$. Let $\mathbf{G}^\alpha$ and $\mathbf{g}^\alpha$ denote the dual (contravariant) tangent vectors of $\mathbf{G}_\alpha$ and $\mathbf{g}_\alpha$, respectively, that is,

$$\mathbf{G}^\alpha \cdot \mathbf{G}_\beta = \mathbf{g}^\alpha \cdot \mathbf{g}_\beta = \delta^\alpha_\beta, \tag{5a,b}$$

where $\delta^\alpha_\beta$ is the Kronecker delta, and $\alpha, \beta \in \{1, 2\}$.

The unit normal vectors to the tangent planes $T_P$ and $T_p$ are given by

$$\mathbf{N} = \frac{\mathbf{G}_1 \times \mathbf{G}_2}{|\mathbf{G}_1 \times \mathbf{G}_2|}, \quad \mathbf{n} = \frac{\mathbf{g}_1 \times \mathbf{g}_2}{|\mathbf{g}_1 \times \mathbf{g}_2|}. \tag{6a,b}$$

The first fundamental form (or the surface metric tensor) $\mathbf{G} = G_{\alpha\beta}\mathbf{G}^\alpha \otimes \mathbf{G}^\beta$, $\mathbf{g} = g_{\alpha\beta}\mathbf{g}^\alpha \otimes \mathbf{g}^\beta$ in the reference and current configurations, respectively, are given by

$$G_{\alpha\beta} = \mathbf{G}_\alpha \cdot \mathbf{G}_\beta, \quad g_{\alpha\beta} = \mathbf{g}_\alpha \cdot \mathbf{g}_\beta. \tag{7a,b}$$

Geometrically, the first fundamental form determines lengths, angles and area on a surface. The contravariant components in the reference and current configurations are given by

$$G^{\alpha\beta} = \mathbf{G}^\alpha \cdot \mathbf{G}^\beta, \quad g^{\alpha\beta} = \mathbf{g}^\alpha \cdot \mathbf{g}^\beta. \tag{8a,b}$$

The second fundamental form (or curvature tensor) $\mathbf{B} \equiv B_{\alpha\beta} \mathbf{G}^\alpha \otimes \mathbf{G}^\beta$, $\mathbf{b} \equiv b_{\alpha\beta} \mathbf{g}^\alpha \otimes \mathbf{g}^\beta$ in the reference and current configurations, respectively, are given by

$$B_{\alpha\beta} = \mathbf{G}_{\alpha,\beta} \cdot \mathbf{N}, \quad b_{\alpha\beta} = \mathbf{g}_{\alpha,\beta} \cdot \mathbf{n}. \tag{9a,b}$$

The mean and Gaussian curvature are one half of the trace and determinant of the second fundamental form.

Using the chain rule, the local basis vectors in the reference and current configurations are related by

$$\mathbf{g}_\alpha = \mathbf{F} \cdot \mathbf{G}_\alpha. \tag{10}$$

A more useful way to describe the deformation of $P \in \partial\Omega_0$ that does not involve the deformation of the bulk solid is to introduce the surface deformation gradient $\mathbf{F}_s$ by

$$\mathbf{F}_s \equiv \nabla_s \mathbf{r} = \mathbf{g}_\alpha \otimes \mathbf{G}^\alpha, \tag{11}$$

where the subscript 's' indicates the corresponding quantity is surface associated, and $\nabla_s$ is defined as the surface gradient by $\nabla_s( \ ) \equiv ( \ )_{,\alpha} \otimes \mathbf{G}^\alpha$. Here the quantity in $( \ )$ can be a scalar, surface vector or surface tensor. It can be readily checked that

$$\mathbf{g}_\alpha = \mathbf{F} \cdot \mathbf{G}_\alpha = \mathbf{F}_s \cdot \mathbf{G}_\alpha. \tag{12}$$

We introduce two commonly used surface tensors for measuring surface deformation: the right surface Cauchy-Green tensor $\mathbf{C}_s$ and the relative curvature tensor $\boldsymbol{\kappa}$. The right surface Cauchy-Green tensor is

$$\mathbf{C}_s = \mathbf{F}_s^\mathrm{T} \cdot \mathbf{F}_s = g_{\alpha\beta} \mathbf{G}^\alpha \otimes \mathbf{G}^\beta, \tag{13}$$

A surface tensor often used in the reference configuration is the *relative curvature tensor* $\boldsymbol{\kappa}$; it is defined by[42]

$$\boldsymbol{\kappa} \equiv -\mathbf{F}_s^\mathrm{T} \cdot \mathbf{b} \cdot \mathbf{F}_s = \kappa_{\alpha\beta} \mathbf{G}^\alpha \otimes \mathbf{G}^\beta \tag{14}$$

where $\kappa_{\alpha\beta} = -b_{\alpha\beta}$. However, it must be noted that in general $\boldsymbol{\kappa} \neq -\mathbf{b}$ since they are associated with different bases. To gain physical insight, consider a curve $C$ in the reference configuration (as shown in Fig. 2); it is mapped by $\chi$ to the curve $c$ in the current configuration. The *unit* tangent vectors to the curves at $P$ and $p$ are denoted as $\mathbf{S}$ and $\mathbf{s}$, respectively. Suppose the curve stretch ratio at $P$ is $\lambda$, that is

$$\lambda\mathbf{s} = \mathbf{F}_s\mathbf{S}. \tag{15a}$$

Since $|\mathbf{s}| = 1$,

$$\lambda^2 = \mathbf{F}_s\mathbf{S} \cdot \mathbf{F}_s\mathbf{S} = \mathbf{S} \cdot \mathbf{F}_s^{\mathrm{T}}\mathbf{F}_s\mathbf{S} = \mathbf{S} \cdot \mathbf{C}_s\mathbf{S} \,. \tag{15b}$$

The normal curvature of the curve $c$ in the current configuration is $\mathbf{s} \cdot \mathbf{bs}$, it is also equal to $-\dfrac{1}{\lambda^2}\mathbf{S} \cdot \boldsymbol{\kappa}\mathbf{S}$ since

$$\mathbf{S} \cdot \boldsymbol{\kappa} \cdot \mathbf{S} = \mathbf{S} \cdot \left(-\mathbf{F}_s^{\mathrm{T}} \cdot \mathbf{b} \cdot \mathbf{F}_s\right) \cdot \mathbf{S} = -\left(\mathbf{F}_s\mathbf{S}\right) \cdot \mathbf{b}\left(\mathbf{F}_s\mathbf{S}\right) = -\left(\lambda\mathbf{s}\right) \cdot \mathbf{b}\left(\lambda\mathbf{s}\right) = -\lambda^2\mathbf{sbs} \tag{16}$$

Therefore $\boldsymbol{\kappa}$ scales the curvature by the square of its local stretch. In other words, $\boldsymbol{\kappa}$ combines both the stretch and curvature change on a surface. In the following, we will illustrate this tensor using a simple example.
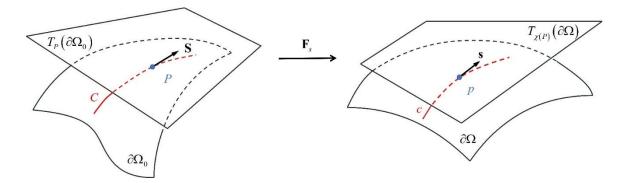


Fig. 2. A schematic of a curve (red line) in the reference and current configurations.

## 2.2 Constitutive law and Equilibrium equations for Elastic Surfaces
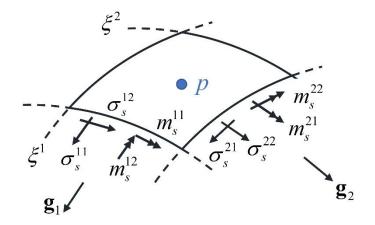


Fig. 3. The components of surface stress and stress bending moment acting on a coordinate neighborhood of material point p (blue point). $\mathbf{g}_1$ and $\mathbf{g}_2$ are tangent vectors to the surface at $p$ and they are not necessarily perpendicular to each other; $\xi^1$ and $\xi^2$ are the curvilinear coordinates. The positive directions of surface

stresses are indicated by simple arrows, and surface bending moments by two-headed arrows following the right-hand rule

We assume that the surface Helmholtz free energy, $A$, is a function of the surface deformation gradient, i.e., that the surface is hyperelastic. The Cauchy (true) surface stress $\boldsymbol{\sigma}_s = \sigma_s^{\alpha\beta} \mathbf{g}_\alpha \otimes \mathbf{g}_\beta$ (with units of force per length) and surface bending moment $\mathbf{m}_s = m_s^{\alpha\beta} \mathbf{g}_\alpha \otimes \mathbf{g}_\beta$ (with units of moment per length) can be obtained through Helmholtz surface energy $A$ by

$$\boldsymbol{\sigma}_s = \frac{2}{J_s} \mathbf{F}_s \frac{\partial A}{\partial \mathbf{C}_s} \mathbf{F}_s^{\mathrm{T}} = \frac{1}{J_s} \frac{\partial A}{\partial \mathbf{F}_s} \mathbf{F}_s^{\mathrm{T}}, \tag{17a}$$

$$\mathbf{m}_s = \frac{1}{J_s} \mathbf{F}_s \frac{\partial A}{\partial \boldsymbol{\kappa}} \mathbf{F}_s^{\mathrm{T}}, \tag{17b}$$

where $J_s = \det(\mathbf{F}_s)$ is the ratio of surface area of a material element in the current and reference configurations.[42] The convention of components' directions is indicated in Fig. 3. Note due to the symmetry of $\mathbf{C}_s$ and $\boldsymbol{\kappa}$, the Cauchy surface stress and surface bending moment are symmetric. If the surface is orientable and isotropic[55], the surface free energy density can be expressed in terms of the six invariants of the right surface Cauchy-Green tensor $\mathbf{C}_s$ and the relative curvature tensor $\boldsymbol{\kappa}$ as

$$A(\mathbf{C}_s, \boldsymbol{\kappa}) = A\left(I_1^s, I_2^s, \mathsf{L} , I_6^s\right), \tag{18a}$$

where

$$I_1^s = \mathrm{tr}(\mathbf{C}_s), \ I_2^s = \det(\mathbf{C}_s), \ I_3^s = \mathrm{tr}(\boldsymbol{\kappa}), \ I_4^s = \det(\boldsymbol{\kappa}), \ I_5^s = \mathrm{tr}(\mathbf{C}_s \cdot \boldsymbol{\kappa}), \ I_6^s = \mathrm{tr}(\mathbf{C}_s \cdot \boldsymbol{\kappa} \cdot \boldsymbol{\Psi}), \tag{18b-g}$$

and $\boldsymbol{\Psi} = \Psi^{\alpha\beta} \mathbf{G}_\alpha \otimes \mathbf{G}_\beta$ is the anti-symmetric surface permutation tensor in the reference configuration satisfying $\Psi^{\alpha\beta} \sqrt{\det(G_{\alpha\beta})} = e^{\alpha\beta}$, $e^{12} = -e^{21} = 1$, $e^{11} = e^{22} = 0$. Also, $J_s$ is often used in some literature instead of $I_2^s$, since $I_2^s = J_s^2$. By equations (17a,b) and (18a,b), the surface stress and moment are[43]

$$\boldsymbol{\sigma}_s = \frac{2}{J_s} \left[ \frac{\partial A}{\partial I_1^s} \mathbf{B}_s + \frac{J_s}{2} \frac{\partial A}{\partial J_s} \mathbf{1}_s - \frac{\partial A}{\partial I_5^s} \mathbf{B}_s \mathbf{b} \mathbf{B}_s + \frac{J_s}{2} \frac{\partial A}{\partial I_6^s} (\boldsymbol{\psi} \mathbf{b} \mathbf{B}_s - \mathbf{B}_s \mathbf{b} \boldsymbol{\psi}) \right] \tag{19a}$$

$$\mathbf{m}_s = \frac{1}{J_s} \left[ \frac{\partial A}{\partial I_3^s} \mathbf{B}_s - I_4 \frac{\partial A}{\partial I_4^s} \mathbf{b}^{-1} + \frac{\partial A}{\partial I_5^s} \mathbf{B}_s^2 + \frac{J_s}{2} \frac{\partial A}{\partial I_6^s} (\boldsymbol{\psi} \mathbf{B}_s - \mathbf{B}_s \boldsymbol{\psi}) \right] \tag{19b}$$

where $\mathbf{B}_s = \mathbf{F}_s\mathbf{F}_s^{\mathrm{T}}$ is the *left surface Cauchy-Green tensor*, $\mathbf{1}_s$ is the surface identity tensor, and $\boldsymbol{\psi} = \psi^{\alpha\beta}\mathbf{g}_\alpha \otimes \mathbf{g}_\beta$ is surface permutation tensor in the current configuration. In the following, we consider a special and simple case where $A$ is independent of $I_4^s$, $I_5^s$ and $I_6^s$. Particularly, $I_4^s$ is zero for surfaces with one principal curvature being zero (e.g., in plane strain problems), while $I_5^s$ and $I_6^s$ represent more complicated surface behaviors coupling $\mathbf{C}_s$ and $\boldsymbol{\kappa}$. For this case, (19a,b) reduces to

$$\boldsymbol{\sigma}_s = \frac{2}{J_s}\frac{\partial A}{\partial I_1^s}\mathbf{B}_s + \frac{\partial A}{\partial J_s}\mathbf{1}_s \tag{19c}$$

$$\mathbf{m}_s = \frac{1}{J_s}\frac{\partial A}{\partial I_3^s}\mathbf{B}_s \tag{19d}$$

**2.3 Interpretation of material constants in a simple surface constitutive model**

To gain insight, consider a simple surface Helmholtz free energy which depends only on $I_1^s$, $I_2^s$ (or $J_s$ equivalently) and $I_3^s$. Specifically,

$$A\left(I_1^s, J_s, I_3^s\right) = a_1\left(I_1^s - 2\right) + a_2\left(J_s - 1\right) + \frac{a_3}{2}\left(J_s - 1\right)^2 + \frac{a_4}{2}\left[I_3^s - I_3^s(0)\right]^2, \tag{20}$$

where $I_3^s(0)$ is the trace of $\boldsymbol{\kappa}$ in the reference configuration, and $a_i$'s ($i$ =1-4) are material properties which we shall interpret below. The physical meaning of each $a_i$ can be understood by virtual experiments. First, we consider a simple surface shear experiment. The surface originally lies in the *x-y* plane with coordinates $X_1$ and $X_2$ associated with an orthonormal basis $\{\mathbf{e}_1, \mathbf{e}_2\}$. $X_1$ and $X_2$ are the curvilinear coordinates in this case. The position in the reference configuration is $\mathbf{R} = X_1\mathbf{e}_1 + X_2\mathbf{e}_2$, and after deformation is $\mathbf{r} = \left(X_1 + \gamma X_2\right)\mathbf{e}_1 + X_2\mathbf{e}_2$ (Fig. 4). The surface deformation gradient is

$$\mathbf{F}_s = \mathbf{e}_1 \otimes \mathbf{e}_1 + \mathbf{e}_2 \otimes \mathbf{e}_2 + \gamma\mathbf{e}_1 \otimes \mathbf{e}_2 \tag{21}$$

Using equation (19c) the Cauchy surface stress is

$$\boldsymbol{\sigma}_s = 2a_1\mathbf{B}_s + a_2\mathbf{1}_s \tag{22a}$$

where $\mathbf{B}_s = \left(1+\gamma^2\right)\mathbf{e}_1 \otimes \mathbf{e}_1 + \gamma\mathbf{e}_1 \otimes \mathbf{e}_2 + \gamma\mathbf{e}_2 \otimes \mathbf{e}_1 + \mathbf{e}_2 \otimes \mathbf{e}_2$ and we have used $J_s = \det\left(\mathbf{F}_s\right) = 1$. In component form, the surface tensor is

$$[\boldsymbol{\sigma}_s] = \begin{bmatrix} 2a_1 + a_2 & 0 \\ 0 & 2a_1 + a_2 \end{bmatrix} + 2a_1 \begin{bmatrix} 0 & \gamma \\ \gamma & 0 \end{bmatrix} + 2a_1 \begin{bmatrix} \gamma^2 & 0 \\ 0 & 1 \end{bmatrix} \tag{22b}$$

Here the notation $[\ ]$ denotes the matrix of the components of a tensor. The surface stress contains a *constant isotropic part* $(2a_1 + a_2)\mathbf{1}_s$. Thus, the sum $\sigma_0 \equiv 2a_1 + a_2$ can be interpreted as a constant isotropic surface stress. We shall call $\sigma_0 \equiv 2a_1 + a_2$ as the *zero-strain or residual surface stress*. For $\gamma$ small but non-zero, the shear stress is proportional to $2a_1$ thus $G_s \equiv 2a_1$ is the *small strain surface shear modulus*.



$$\mathbf{R} = X_1 \mathbf{e}_1 + X_2 \mathbf{e}_2 \qquad\qquad \mathbf{r} = (X_1 + \gamma X_2)\mathbf{e}_1 + X_2 \mathbf{e}_2$$
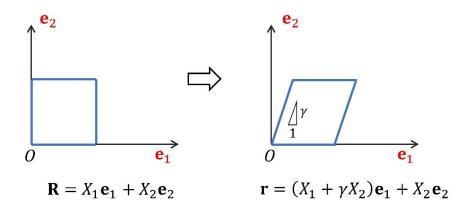
Fig. 4. Schematic of a simple shear test of a surface element.

Consider another example where the surface is subjected to a uniform biaxial stretch with stretch ratios $\lambda_1$ and $\lambda_2$ respectively. The surface deformation gradient is

$$\mathbf{F}_s^{\text{Stretch}} = \lambda_1 \mathbf{e}_1 \otimes \mathbf{e}_1 + \lambda_2 \mathbf{e}_2 \otimes \mathbf{e}_2 \tag{23}$$

The surface stress computed using (19c) and (20) is, after some rearrangement:

$$[\boldsymbol{\sigma}_s] = \sigma_0 \begin{bmatrix} 1 & 0 \\ 0 & 1 \end{bmatrix} + G_s \begin{bmatrix} \lambda_1/\lambda_2 - 1 & 0 \\ 0 & \lambda_2/\lambda_1 - 1 \end{bmatrix} + a_3 \begin{bmatrix} J_s - 1 & 0 \\ 0 & J_s - 1 \end{bmatrix} \tag{24}$$

Consistent with the simple shear test, the first term is the residual isotropic surface stress. The second non-isotropic term vanishes if $\lambda_1 = \lambda_2$, that is, when the surface is subjected to a hydrostatic strain. The third term indicates that $a_3$ is related to surface compressibility, i.e., $\sigma_s^{11} + \sigma_s^{22}$ increases linearly with the change in surface area strain with slope $2a_3$. In analogy with linear elasticity, $K_s \equiv a_3$ is the surface area modulus.

More connection with linear elasticity can be made by consider the special case of a uniaxial tension test. Here we prescribe $\lambda_1$ and $\lambda_2$ is determined by the condition that $\sigma_s^{22} = 0$. Assuming small deformation so that

$\lambda_1 = 1 + \varepsilon_{11}, \lambda_2 = 1 + \varepsilon_{22}$ where $|\varepsilon_{11}|, |\varepsilon_{22}| \ll 1$. Ignoring the residual stress term, the condition that $\sigma_s^{22} = 0$ implies that

$$G_s \left( \varepsilon_{22} - \varepsilon_{11} \right) + K_s \left( \varepsilon_{22} + \varepsilon_{11} \right) = 0 \Rightarrow \frac{\varepsilon_{22}}{\varepsilon_{11}} = -\left( \frac{K_s - G_s}{K_s + G_s} \right), \tag{25}$$

where we have used that $\lambda_2 / \lambda_1 = (1 + \varepsilon_{22}) / (1 + \varepsilon_{11}) \approx 1 + \varepsilon_{22} - \varepsilon_{11}$. In analogy with linear elasticity, we define the surface Poisson's ratio $\nu_s$ by

$$\nu_s \equiv \left( \frac{K_s - G_s}{K_s + G_s} \right), \tag{26a}$$

and accordingly,

$$K_s = \frac{1 + \nu_s}{1 - \nu_s} G_s \tag{26b}$$

Further, still ignoring the residual term in (24), we find

$$\sigma_s^{11} = G_s \left( \varepsilon_{11} - \varepsilon_{22} \right) + K_s \left( \varepsilon_{11} + \varepsilon_{22} \right) = \left[ G_s \left( 1 + \nu_s \right) + K_s \left( 1 - \nu_s \right) \right] \varepsilon_{11}. \tag{27}$$

Equation (27) motivates us to define a surface tensile modulus $E_s$ by $\sigma_s^{11} \equiv E_s \varepsilon_{11}$. Comparing this definition with (27), the surface tensile modulus is related to the surface shear modulus and the surface Poisson's ratio by

$$E_s = G_s \left( 1 + \nu_s \right) + K_s \left( 1 - \nu_s \right) = 2 G_s \left( 1 + \nu_s \right), \tag{28}$$

where we have used (26b) in the last step of (28). It is interesting to note that the relation between surface shear and tensile modulus is the same as in linear elasticity. A more formal approach (see Electronic supplementary information (ESI)) shows that, in the *small strain* limit, (19c) reduces to

$$\sigma_{\alpha\beta} = 2 G_s \varepsilon_{\alpha\beta} + \left( K_s - G_s \right) \varepsilon_{\gamma\gamma} \delta_{\alpha\beta} + \sigma_0 \delta_{\alpha\beta} \tag{29a}$$

From (29a), the surface Lame's constant is

$$\Lambda_s = K_s - G_s. \tag{29b}$$

Here we note that Style et al.[4] suggest that $\Lambda_s = K_s - 2G_s / 3$, which is the same as in bulk elasticity. However, our approach shows that $\Lambda_s = K_s - G_s$; indeed, the factor of 3 in the denominator of $2G_s / 3$ should be replaced by 2 as the surface is 2D.

Next we investigate the physical meaning of $a_4$. This constant does not appear in the analysis above since the surface remains flat during deformation. To understand $a_4$ we consider pure bending. As shown in Fig. 5, the surface is initially flat (i.e., curvature tensor is zero) in the $\mathbf{e}_1$ and $\mathbf{e}_2$ directions, then it is bent to be part of a circular cylinder with a radius $a$. The basis for the reference configuration is chosen to be $\{\mathbf{e}_1, \mathbf{e}_2\}$. During pure bending, $\mathbf{e}_1$ remains unchanged while $\mathbf{e}_2$ is mapped to $\mathbf{s}$ in the current configuration, where $\mathbf{s}$ is the unit tangent vector to the surface and $\mathbf{e}_1 \perp \mathbf{s}$ (see Fig. 5). The basis for the current configuration is then $\{\mathbf{e}_1, \mathbf{s}\}$ The surface deformation gradient tensor for pure bending is
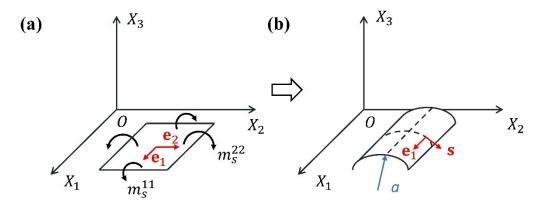


Fig. 5. Schematic of a surface to be stretched biaxially and bent to part of a cylinder surface.

$$\mathbf{F}_s^{\text{Bend}} = \mathbf{e}_1 \otimes \mathbf{e}_1 + \mathbf{s} \otimes \mathbf{e}_2 \tag{30}$$

The second fundamental form of the deformed cylinder surface is

$$\mathbf{b} = -\frac{1}{a} \mathbf{s} \otimes \mathbf{s} \tag{31}$$

Note, since the normal vector to the sphere is assumed to be outward, the curvature is negative. Using (19c,d) and (20), the surface stress and surface bending moment are

$$\boldsymbol{\sigma}_s = \sigma_0 \mathbf{1}_s \tag{32a}$$

$$\mathbf{m}_s = \frac{a_4}{a} \mathbf{1}_s \tag{32b}$$

where we have used $\mathbf{1}_s = \mathbf{e}_1 \otimes \mathbf{e}_1 + \mathbf{s} \otimes \mathbf{s}$ in (32a,b). Recall that in pure bending of an elastic beam, the bending moment is directly proportional to the curvature with the proportionality constant being the bending stiffness. Thus, $a_4 \equiv D_s$ should be interpreted as the *surface bending stiffness*. In this model pure bending has no effect

12

on the surface stress, since it does not introduce surface strains.  Note also that the bending moment for pure bending is the same in both $\mathbf{e}_1$ and $\mathbf{s}$ direction.

In summary, the true stress and moment associated with the surface free energy given by (20) is related to the left-Cauchy Green surface tensor $\mathbf{B}_s$ and the trace of the relative curvature tensor $\boldsymbol{\kappa}$ by

$$\boldsymbol{\sigma}_s = \sigma_0 \mathbf{1}_s + G_s \left[ \frac{\mathbf{B}_s}{J_s} - \mathbf{1}_s \right] + K_s \left( J_s - 1 \right) \mathbf{1}_s \tag{33a}$$

$$\mathbf{m}_s = \frac{D_s \left( I_3^s - I_3^s (0) \right)}{J_s} \mathbf{B}_s \tag{33b}$$

We end this section with an example motivating the relative curvature tensor. Recall this tensor takes into account that curves on the surface are stretched, i.e., arclengths change due to surface deformation.  To see how stretching is incorporated into this tensor, consider an initially flat surface subjected to a bi-axial stretch.  This biaxial stretching is followed by a pure bending resulting in a circular cylindrical surface of radius $a$.  The surface deformation gradient associated with this deformation sequence is simply $\mathbf{F}_s = \mathbf{F}_s^{\text{Bend}} \mathbf{F}_s^{\text{stretch}}$.  Using (23) and (30), this is:

$$\mathbf{F}_s = \mathbf{F}_s^{\text{Bend}} \mathbf{F}_s^{\text{stretch}} = \lambda_1 \mathbf{e}_1 \otimes \mathbf{e}_1 + \lambda_2 \mathbf{s} \otimes \mathbf{e}_2 \tag{34}$$

The curvature tensor is still given by (31).   The surface stress and moment are:

$$\boldsymbol{\sigma}_s = \sigma_0 \mathbf{1}_s + G_s \left[ \left( \frac{\lambda_1}{\lambda_2} - 1 \right) \mathbf{e}_1 \otimes \mathbf{e}_1 + \left( \frac{\lambda_2}{\lambda_1} - 1 \right) \mathbf{s} \otimes \mathbf{s} \right] + K_s \left( J_s - 1 \right) \mathbf{1}_s \tag{35a}$$

$$\mathbf{m}_s = \frac{D_s}{a} \left[ \lambda_1 \lambda_2 \mathbf{e}_1 \otimes \mathbf{e}_1 + \frac{\lambda_2^3}{\lambda_1} \mathbf{s} \otimes \mathbf{s} \right] \tag{35b}$$

Equation (35b) states that *bending is coupled* to surface shear and stretch.  For example, the first term in (35b) shows that stretching increases bending moment in the $\mathbf{e}_1$ direction.   However, in the $\mathbf{s}$ direction, stretching in the $\mathbf{e}_1$ direction can cause the bending moment to decrease.  Further, bending becomes extremely difficult for large $\lambda_2$ since the moment increases as the third power of $\lambda_2$.  From (35b), it is seen that ratio of the bending moment $m_s^{22} / m_s^{11}$ increases quadratically with the ratio of the stretch ratios, i.e.,

$$m_s^{22} / m_s^{11} = \left( \lambda_2 / \lambda_1 \right)^2 \tag{36}$$

**2.4 Surface Equilibrium Equations or Balance Laws for Quasi-static or Static problems**

The external moments and force acting on a surface must be balanced. In quasi-statics problems where inertia effects can be ignored, the surface equilibrium equation is[43]

$$\left[\boldsymbol{\sigma}\right]_{-}^{+} \cdot \mathbf{n} = -\nabla_s \cdot \left[\left(\boldsymbol{\sigma}_s - \mathbf{b} \cdot \mathbf{m}_s\right) + \mathbf{n} \otimes \left(\mathbf{D} \cdot \mathbf{m}_s\right)\right], \tag{37}$$

where $\nabla_s \cdot (\;) \equiv \dfrac{\partial (\;)}{\partial \xi^\alpha} \cdot \mathbf{g}^\alpha$ is the surface divergence, and $\mathbf{D}$ is the covariant derivative which drops the normal component of $\nabla_s \cdot (\;)$, i.e., $\mathbf{D} \cdot (\;) \equiv (\mathbf{1} - \mathbf{n} \otimes \mathbf{n}) \cdot \nabla_s \cdot (\;)$. The notation $\left[\boldsymbol{\sigma}\right]_{-}^{+}$ represents the discontinuity of the true stress across the interface in the current configuration. The symbols '+' and '-' are associated with the direction of $\mathbf{n}$ (Fig. 6). For example, if the '+' side of the surface is air (*traction free*) while the '-' side is the bulk, then $\left[\boldsymbol{\sigma}\right]_{-}^{+}$ is the *negative* of true stress tensor in the bulk at the point $p$.
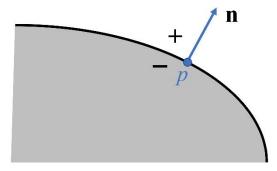


Fig. 6. Stress jump across a surface. The '+' and '-' sides are determined by the direction of normal vector, $\mathbf{n}$, to the surface.

The indicial form of (37) is[42,45] (see also ESI)

$$\left(\sigma_s^{\alpha\beta} - m_s^{\alpha\gamma} b^\beta{}_\gamma\right) b_{\alpha\beta} + m_s^{\beta\alpha}{}_{|\alpha\beta} + \left[\sigma\right]_{-}^{+\,33} = 0 \tag{38a}$$

$$\left(\sigma_s^{\alpha\beta} - m_s^{\alpha\gamma} b^\beta{}_\gamma\right)_{|\alpha} - b_\gamma^\beta m_s^{\gamma\alpha}{}_{|\alpha} + \left[\sigma\right]_{-}^{+\,\beta 3} = 0 \tag{38b}$$

where $b^\alpha{}_\beta = g^{\alpha\gamma} b_{\gamma\beta}$, and a single stroke '|' means covariant differentiations, and the superscript 3 indicates the $\mathbf{n}$ direction. For completeness, we include details on surface differentiation such as surface divergence and covariant derivatives in the ESI.

**2.5 Special 2D plane strain problems**

The formulation presented above is quite general. Here we specialize to 2D plane-strain problems where the surface in the reference and deformed configuration is cylindrical and the deformation out of plane (unit vector $\mathbf{v}$ direction, see Fig. 7) is zero. Specifically, these surfaces are generated by translating a curve $C$ (reference configuration) or its image $c$ (deformed configuration) in the out of plane direction. and the deformation out of plane (unit vector $\mathbf{v}$ direction, see Fig. 7) is zero. Specifically, the surface stretch ratio out-of-plane is exactly one, so $J_s$ is the same as the in-plane stretch ratio $\lambda_s$. The curve $c$ will be parameterized by its arc length $s$. This parameterization introduces a unit tangent vector, i.e., $\mathbf{g}_1 = \mathbf{s}$. The other basis vector $\mathbf{g}_2$ is the bi-normal vector $\mathbf{v} = \mathbf{n} \times \mathbf{s} \equiv \mathbf{g}_2$ where $\mathbf{n}$ is the unit normal to $c$. The surface deformation gradient tensor is $\mathbf{F}_s = \lambda_s \mathbf{s} \otimes \mathbf{S} + 1\mathbf{v} \otimes \mathbf{v}$, where $\mathbf{S}$ is the unit tangent vector in the reference configuration and we have used $\mathbf{v} = \mathbf{V}$ due to the plane strain assumption. Using $\mathbf{1}_s = \mathbf{s} \otimes \mathbf{s} + \mathbf{v} \otimes \mathbf{v}$ and $\mathbf{F}_s \mathbf{F}_s^{\mathrm{T}} = \lambda_s^2 \mathbf{s} \otimes \mathbf{s} + \mathbf{v} \otimes \mathbf{v}$, the true surface stress and surface bending moment with the free energy given by (20) are

$$\boldsymbol{\sigma}_s = \left[\sigma_0 + E_s^*\left(\lambda_s - 1\right)\right]\mathbf{s} \otimes \mathbf{s} + \left[\sigma_0 + G_s\left(\lambda_s^{-1} - 1\right) + K_s\left(\lambda_s - 1\right)\right]\mathbf{v} \otimes \mathbf{v}, \tag{39a}$$

$$\mathbf{m}_s = D_s\left[I_3^s - I_3^s\left(0\right)\right]\left[\lambda_s \mathbf{s} \otimes \mathbf{s} + \frac{1}{\lambda_s}\mathbf{v} \otimes \mathbf{v}\right], \tag{39b}$$

where $E_s^* \equiv G_s + K_s = \dfrac{2G_s}{1 - v_s} = \dfrac{E_s}{1 - v_s^2}$ is the plane strain tensile modulus.

With respect to the *orthonormal* basis $\{\mathbf{s}, \mathbf{v}, \mathbf{n}\}$ the only non-trivial component of the second fundamental form is $b_{11}$ (and $b_{11} = b^1{}_1$), and it is the in-plane curvature of the deformed curve $c$. We denote it by $h$ which can be positive or negative depends on the parameterization and normal vector direction. A simple way to calculate the in-plane curvature $h$ is

$$h = \frac{\partial \mathbf{s}}{\partial s} \cdot \mathbf{n} \tag{40}$$

The trace of the relative curvature tensor in plane strain is

$$I_3^s = -\lambda_s^2 h \tag{41}$$

Due to the plane strain assumption and the arc length parameterization, the out of plane surface equilibrium equation is automatically satisfied, and we need only to enforce in-plane equilibrium (details of derivation are provided in the ESI). Equations (38a,b) reduce to

$$\left(\sigma_s^{11} - m_s^{11}h\right)h + m_s^{11}{}_{,11} + \left[\sigma^{33}\right]_-^+ = 0 \tag{42a}$$

15

$$\left(\sigma_s^{11}-m_s^{11}h\right)_{,1}-hm_{s}^{11}{}_{,1}+\left[\sigma^{13}\right]_-^+=0 \tag{42b}$$

where

$$\sigma_s^{11}=\sigma_0+E_s^*\left(\lambda_s-1\right) \tag{42c}$$

$$m_s^{11}=\lambda_s D_s\left[I_3^s-I_3^s\left(0\right)\right] \tag{42d}$$

and $_{,1}$ denotes partial derivative with respect to arc length $s$. Using (41), (42d) can be expressed as

$$m_s^{11}=-\lambda_s D_s\left(\lambda_s^2 h-h_0\right) \tag{42e}$$
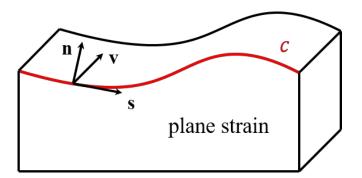
where $h_0$ is the initial in-plane curvature.



Fig. 7. Schematic shows the plane strain problem in which the surface is cylindrical, generated by translating the red curve $c$ in the $\mathbf{v}$ direction (out of plane). Here $\{\mathbf{s}, \mathbf{v}, \mathbf{n}\}$ is an orthonormal basis: $\mathbf{s}, \mathbf{v}, \mathbf{n}$ are unit tangent, binormal and normal vectors in the deformed configuration, respectively. Not shown is the reference configuration.

## 3. Inflation of a hyperelastic cylindrical shell

### 3.1 Problem statement and solution

In the first example, we study the effects of surface stress and bending on the inflation of a cylindrical shell made of an incompressible isotropic hyperelastic material. This class of problems has been well studied by many;[52,56–63] here we focus on surface stress and bending effects. In this problem, the undeformed configuration corresponds to a stress-free cylindrical shell without surface stress or surface bending moment. Let $\left(R,\Theta\right)$ identify a material point in the reference configuration, and $\left(r,\theta\right)$ its current configuration. The

inner surface is inflated by a uniform pressure $\mathbf{T} = -T\mathbf{e}_r$ and no traction is applied on the outer surface. We consider cylindrically symmetric deformation where material points move radially, i.e.,

$$r = r(R), \quad \theta = \Theta. \tag{43}$$

The basis for the reference and deformed configuration can be chosen as $\{\mathbf{e}_r, \mathbf{e}_\theta\}$ which is the standard basis associated with a polar coordinate system with origin at the center of the shell. Before deformation the inner and outer radii are denoted by $R_A$ and $R_B$; and after deformation, by $r_A$ and $r_B$ (see Fig. 8). We use a parameter $f = R_A / R_B$ to represent the shell's thickness. Both the inner and outer surfaces carry a strain-dependent surface stress and bending moment given by (42c,d). The bulk of the cylindrical shell is modeled as an incompressible neo-Hookean solid with strain energy density function

$$W = \frac{\mu}{2}(I_1 - 3), \tag{44}$$

where $I_1$ is the trace of the right Cauchy-Green tensor $\mathbf{C} = \mathbf{F}^T\mathbf{F}$, and $\mu$ is the small strain shear modulus. Because of symmetry, the only non-trivial stresses are the true radial and circumferential stresses and they are denoted by $\sigma_{rr}$ and $\sigma_{\theta\theta}$, respectively.
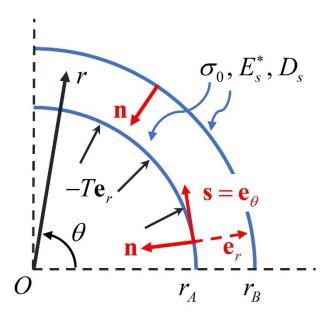


Fig. 8 Current configuration of a cylindrical shell with finite thickness. Its bulk is modeled as neo-Hookean material. The inner surface at $r = r_A$ is subject to a uniform pressure, and both surfaces at $r = r_A$ and $r = r_B$ (blue solid curves) carry surface stresses and surface bending moments. $\mathbf{e}_r$, $\mathbf{e}_\theta$ are the canonical basis vectors in

polar coordinates, and $\mathbf{s}$, $\mathbf{n}$ are the unit tangent and normal vectors for the inner surface. In our system, $\mathbf{s}$ and $\mathbf{e}_\theta$ are the same, while $\mathbf{n}$ and $\mathbf{e}_r$ are equal and opposite.

We normalize all positions by $R_A$ and stresses by $\mu$. Specifically, $\bar{r} \equiv r / R_A$, $\bar{\sigma}_{rr} \equiv \sigma_{rr} / \mu$, $\bar{\sigma}_{\theta\theta} \equiv \sigma_{\theta\theta} / \mu$, and $\bar{T} \equiv T / \mu$. We define the elasto-capillary number by $\bar{\sigma}_0 \equiv \sigma_0 / \mu R_A$, elasto-bending number by $\bar{D}_s \equiv (D_s / \mu)^{1/3} / R_A$, and elasto-stiffening number by $\bar{E}_s^* \equiv E_s^* / \mu R_A$. The stretch ratio of the inner surface $\lambda_A = r_A / R_A$ is related to the applied normalized pressure $\bar{T}$ by the nonlinear equation:

$$
\bar{T} = \frac{1}{2}\left[ 2\ln\frac{\lambda_A}{\sqrt{1+\left(\lambda_A^2-1\right)f^2}} + \frac{1}{1+\left(\lambda_A^2-1\right)f^2} - \frac{1}{\lambda_A^2} \right] + \bar{\sigma}_0\left[ \frac{1}{\lambda_A} + \frac{f}{\sqrt{1+\left(\lambda_A^2-1\right)f^2}} \right]
$$
$$
+\bar{E}_s^*\left[ \frac{\lambda_A-1}{\lambda_A} + \frac{\left(\sqrt{1+\left(\lambda_A^2-1\right)f^2}-1\right)f}{\sqrt{1+\left(\lambda_A^2-1\right)f^2}} \right] + \bar{D}_s^3\left[ \frac{\lambda_A-1}{\lambda_A} + \frac{\left(\sqrt{1+\left(\lambda_A^2-1\right)f^2}-1\right)f^3}{\sqrt{1+\left(\lambda_A^2-1\right)f^2}} \right].
$$

$$(45)$$

The normalized true stress $\bar{\sigma}_{rr}$ and $\bar{\sigma}_{\theta\theta}$ are

$$
\bar{\sigma}_{rr} = \frac{1}{2}\left[ \ln\left(\frac{\bar{r}^2-\lambda_A^2+1}{\bar{r}^2}\right) - \frac{\lambda_A^2}{\bar{r}^2} + \frac{1}{\bar{r}^2} \right] + \frac{\bar{\sigma}_0}{\lambda_A} + \frac{\left(\bar{E}_s^* + \bar{D}_s^3\right)\left(\lambda_A-1\right)}{\lambda_A} - \frac{1}{2}\left( 2\ln\frac{1}{\lambda_A} - 1 + \frac{1}{\lambda_A^2} \right) - \bar{T} \qquad (46a)
$$

$$
\bar{\sigma}_{\theta\theta} = \frac{1}{2}\left[ \ln\left(\frac{\bar{r}^2-\lambda_A^2+1}{\bar{r}^2}\right) - \frac{\lambda_A^2}{\bar{r}^2} + \frac{1}{\bar{r}^2} \right] - \frac{\bar{r}^2-\lambda_A^2+1}{\bar{r}^2} + \frac{\bar{r}^2}{\bar{r}^2-\lambda_A^2+1}
$$
$$
+ \frac{\bar{\sigma}_0}{\lambda_A} + \frac{\left(\bar{E}_s^* + \bar{D}_s^3\right)\left(\lambda_A-1\right)}{\lambda_A} - \frac{1}{2}\left( 2\ln\frac{1}{\lambda_A} - 1 + \frac{1}{\lambda_A^2} \right) - \bar{T}.
$$

$$(46b)$$

Thus, once $\lambda_A$ is determined by solving (45), the stress distribution can be determined using (46a,b). Details are given in the ESI. In classical theory, $\bar{\sigma}_0 = \bar{E}_s^* = \bar{D}_s = 0$, and the solution can be found in the textbook by Bower.[64]

## 3.2 Numerical results

We first plot the normalized pressure $\bar{T}$ versus the inner surface stretch ratio $\lambda_A$ for different shell thicknesses $f$ without any surface effects ($\bar{\sigma}_0 = \bar{E}_s^* = \bar{D}_s = 0$). Equation (45) shows that for this case the normalized pressure approaches a finite limit $\bar{T}_\infty = -\ln f$ when the inner surface stretch ratio $\lambda_A \to \infty$. Notice $\bar{T}_\infty$ becomes infinite as $f \to 0$. This particular behavior is different from its 3D counterpart: it is well known

that a pressurized spherical cavity in an *infinite* neo-Hookean solid expands without bound when the pressure approaches $5\mu/2$[58].
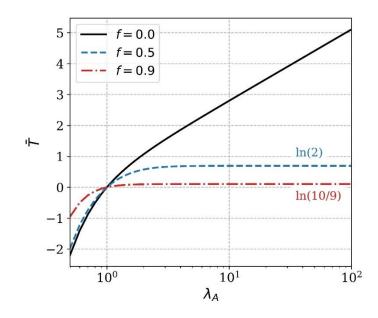


Fig. 9. Normalized pressure versus inner surface stretch ratio with different shell thicknesses. $f = 0$ corresponds to a pressurized cylindrical cavity in an infinite 2D space. No surface effects are considered in this plot.

In the following, we choose $f = 0.9$ to represent a thin cylindrical shell. We study the effect of residual surface stress $(\bar{\sigma}_0)$ first without considering surface stiffening or surface bending effects. In Fig. 10, the filled squares represent the constricted inner surface stretch ratio ($\lambda_A < 1$) when no pressure is applied ($\bar{T} = 0$). As expected, the cylindrical shell shrinks more as $\bar{\sigma}_0$ increases. With increasing pressure, the shell size (both inner and outer radii) starts to grow. However, the pressure attains its maximum value $\bar{T}_{max}$ at a finite value of inner surface stretch ratio (filled circles in Fig. 10). After this, the shell becomes unstable. The reason is that as the cylindrical shell is being inflated, the curvatures on both surfaces decrease. Therefore, the Laplace pressure (the product of residual surface stress and in plane curvature) which opposes the applied pressure decreases and eventually becomes insignificant. Note that the pressure increases monotonically for if the surface residual stress is zero. Thus, surface residue stress is responsible for this unstable behavior.[58,59,61]
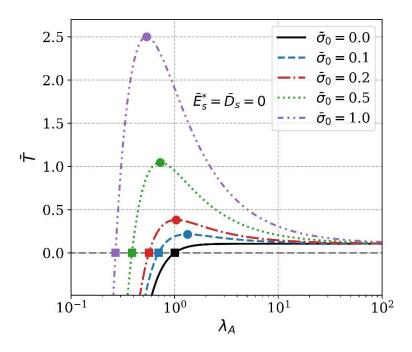
Fig. 10. Normalized pressure versus inner surface stretch ratio for different residual surface stress. The filled squares represent the constricted inner surface stretch ratio because of the residual surface stress provided there is no internal pressure ($\bar{T} = 0$). The filled circles represent the maximal pressure attained during the inflation.

Next, we study surface stiffening and bending effects. Equation (45) shows that the pressure approaches a constant value at $\lambda_A = \infty$, i.e.,

$$\bar{T}_\infty = -\ln(f) + (1+f)\bar{E}_s^* + (1+f^3)\bar{D}_s^3, \tag{47}$$

Fig. 11(a) and (b) demonstrate that for sufficient large surface tensile modulus and bending stiffness, the internal pressure *increases monotonically* with $\lambda_A$; the system is stable (i.e., the maximum pressure $\bar{T}_{max}$ does not exist).

There exist a boundary determined by the combination of $\bar{\sigma}_0$, $\bar{E}_s^*$ and $\bar{D}_s^3$ classifying stable and unstable systems. Fig. 12 plots the boundaries at different $\bar{\sigma}_0$. If the positions of $\bar{E}_s^*$ and $\bar{D}_s^3$ at some given $\bar{\sigma}_0$ are below the corresponding curves, the system then is unstable; otherwise, the system is stable.
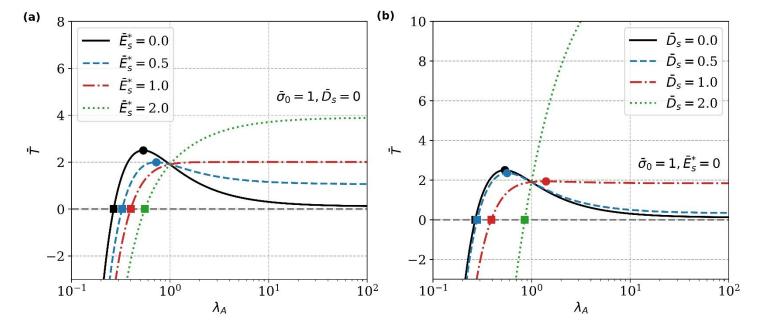
**(a)**



**(b)**

Fig. 11. Normalized pressure versus inner surface stretch ratio for different (a) surface tensile moduli; (b) surface bending stiffnesses. The filled squares represent that there is no internal pressure ($\bar{T} = 0$). The filled circles represent the maximal pressure attained during the inflation.
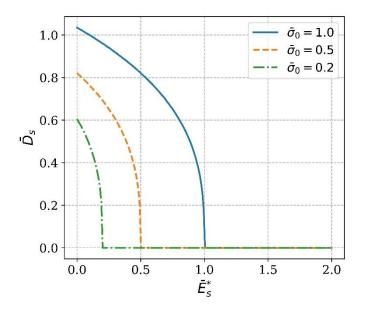


Fig. 12. Boundaries classifying stable and unstable systems at different $\bar{\sigma}_0$.

Fig. 13(a, b) and Fig. 14(a, b) plot the circumferential stress $\sigma_{\theta\theta}$ and radial stress $\sigma_{rr}$ in the bulk at the inner surface versus the inner surface stretch ratio $\lambda_A$. Two cases, $\bar{\sigma}_0$, $\bar{E}_s^* \neq 0$, $\bar{D}_s = 0$ and $\bar{\sigma}_0$, $\bar{E}_s^* = 0$, $\bar{D}_s \neq 0$,

are considered. Using (46b) and the fact that $\bar{T}_\infty$ is finite, the circumference stress on the inner surface becomes unbounded as $\bar{T} \to \bar{T}_\infty$. Indeed,

$$\lim_{\lambda_A \to \infty} \bar{\sigma}_{\theta\theta} \to \lambda_A^2 \tag{48}$$

In a log-log plot, the stress versus stretch curve in this regime should be a straight line with slope 2 and this behavior is shown in Fig. 13(a) and Fig. 14(a). It is interesting to note that for small $\bar{E}_s^*$ or $\bar{D}_s$, the circumferential stress increases monotonically with $\lambda_A$. However, for sufficiently large $\bar{E}_s^*$ or $\bar{D}_s$, the circumferential stress undergoes an oscillation before increasing with the stretch ratio according to (48).

Unlike the circumferential stress, the radial stress remains bounded as $\lambda_A \to \infty$ (Fig. 13(b) and Fig. 14(b)). This asymptotic value of radial stresses is given by:

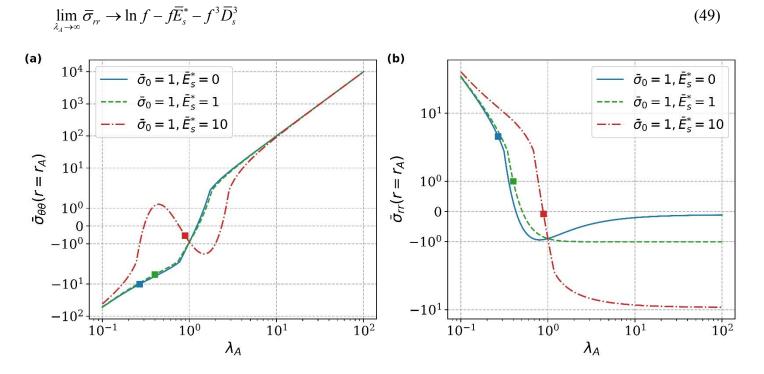$$\lim_{\lambda_A \to \infty} \bar{\sigma}_{rr} \to \ln f - f\bar{E}_s^* - f^3\bar{D}_s^3 \tag{49}$$



Fig. 13. (a) Circumferential and (b) radial stress on the inner surface versus the inner surface stretch ratio with no surface bending stiffness.
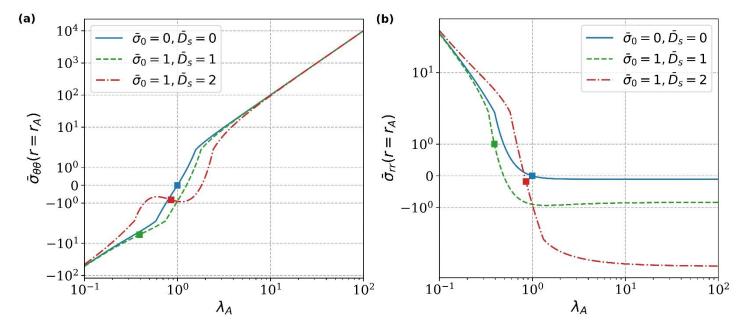
**(a)**

**(b)**

Fig. 14. (a) Circumferential and (b) radial stress on the inner surface versus the inner surface stretch ratio with no surface tensile modulus.

## 4. Bending of a plate with a finite thickness

### 4.1 Problem statement and solution

The undeformed configuration of a plate with a finite thickness is identified by a Cartesian coordinate system with an orthonormal basis $\{\mathbf{E}_1, \mathbf{E}_2\}$. It occupies the region $c_A \leq X_1 \leq c_B$, $-L \leq X_2 \leq L$ and $|X_3| < \infty$ This rectangular cross-section is shown in Fig. 15. Suppose that the plate is bent symmetrically with respect to the $X_1$ axis resulting in a sector of a circular cylindrical shell. The deformed cross-section is defined by a polar coordinate system $(r, \theta)$ with orthogonal basis $\{\mathbf{e}_r, \mathbf{e}_\theta\}$, and it occupies the region $r_A \leq r \leq r_B$, $-\theta_0 \leq \theta \leq \theta_0$. Green and Zerna[65] have shown that for an incompressible elastic material, this deformation can be described by the following mapping

$$r = (2\eta X_1)^{1/2}, \quad \theta = \frac{1}{\eta} X_2, \tag{50}$$

where $\eta$ is an unknown parameter to be determined. Since the plate is not allowed to penetrate itself, $0 < \theta_0 < \pi$. Let $\mathbf{s}, \mathbf{n}$ denote the unit tangent and normal vectors for the curved surfaces (indicated by blue curves in Fig. 15) in the current configuration; $\mathbf{s} = \mathbf{e}_\theta$, $\mathbf{n} = -\mathbf{e}_r$. The applied moment acting on the plate is denoted by $M$, and the in-plane *average* curvature (the curvature of the middle line) is $h = \dfrac{1}{\sqrt{\eta(c_B + c_A)}}$.
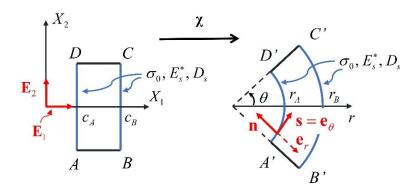
Fig. 15 Rectangular cross-section in the reference and current configurations of a finite thickness plate. This structure is modeled as neo-Hookean material. The surfaces (indicated by blue curves) carry surface stress and surface bending.

We define elasto-capillary number $\bar{\sigma}_0 \equiv \dfrac{\sigma_0}{\mu(c_B - c_A)}$, elasto-bending number $\bar{D}_s \equiv \dfrac{(D_s/\mu)^{1/3}}{c_B - c_A}$, and elasto-stiffening number $\bar{E}_s^* \equiv \dfrac{E_s^*}{\mu(c_B - c_A)}$. We normalize all lengths by $c_B - c_A$, and all stresses by $\mu$, i.e.,

$\bar{c}_A \equiv \dfrac{c_A}{c_B - c_A}$, $\bar{c}_B \equiv \dfrac{c_B}{c_B - c_A} = \bar{c}_A + 1$, $\bar{\eta} \equiv \dfrac{\eta}{c_B - c_A}$, $\bar{r} \equiv \dfrac{r}{c_B - c_A}$, $\bar{\sigma}_{rr} \equiv \dfrac{\sigma_{rr}}{\mu}$ and $\bar{\sigma}_{\theta\theta} \equiv \dfrac{\sigma_{\theta\theta}}{\mu}$. The normalized radial and circumferential true stresses are (details of derivation are in ESI)

$$\bar{\sigma}_{rr} = \frac{\bar{\eta}^2}{2\bar{r}^2} + \frac{\bar{r}^2}{2\bar{\eta}^2} + \bar{C}_2, \quad \bar{\sigma}_{\theta\theta} = -\frac{\bar{\eta}^2}{2\bar{r}^2} + \frac{3\bar{r}^2}{2\bar{\eta}^2} + \bar{C}_2 \tag{51a}$$

where

$$\bar{C}_2 = -\frac{1}{\sqrt{2\bar{\eta}\bar{c}_B}}\left[\bar{\sigma}_0 + \bar{E}_s^*\left(\sqrt{\frac{2\bar{c}_B}{\bar{\eta}}} - 1\right) + \frac{\bar{D}_s^3}{\bar{\eta}^2}\sqrt{\frac{2\bar{c}_B}{\bar{\eta}}}\right] - \frac{\bar{\eta}}{4\bar{c}_B} - \frac{\bar{c}_B}{\bar{\eta}} \tag{51b}$$

The unknown parameter $\bar{\eta}$ is determined by

$$\frac{\bar{c}_B - \bar{c}_A}{\bar{\eta}} - \frac{\bar{\eta}}{4}\left(\frac{1}{\bar{c}_A} - \frac{1}{\bar{c}_B}\right) = \left(\frac{\bar{E}_s^*}{\sqrt{2\bar{\eta}}} - \frac{\bar{\sigma}_0}{\sqrt{2\bar{\eta}}}\right)\left(\frac{1}{\sqrt{\bar{c}_B}} + \frac{1}{\sqrt{\bar{c}_A}}\right) - \frac{2\bar{E}_s^*}{\bar{\eta}} - \frac{2\bar{D}_s^3}{\bar{\eta}^3} \tag{51c}$$

The normalized applied moment and normalized average in-plane curvature are related to each other by

$$\bar{M} \equiv \frac{M}{\mu(c_B - c_A)^2} = -\frac{\bar{\eta}^2}{4}\ln\frac{\bar{c}_B}{\bar{c}_A} - \frac{(\bar{c}_B + \bar{c}_A)}{2} - \bar{\eta}\bar{C}_2 \tag{52a}$$

$$\bar{h} = \frac{1}{\sqrt{\bar{\eta}(\bar{c}_B + \bar{c}_A)}} \tag{52b}$$

## 4.2 Numerical results

We first consider the limiting cases in which the surface bending effect is negligible ($\bar{D}_s = 0$). This problem was studied by Liu et al.[66] In Fig. 16, we plot the applied moment versus average in-plane curvature using equations (52a,b), and Liu et al's results are plotted as symbols for comparison. It is evident that the two solutions agree well. Before we dive into our analysis taking surface bending into account, we review some key findings:

(i) The residual surface stress increases the structural bending resistance – for a given average in-plane curvature, a larger applied bending moment is needed in the presence of residual surface stress.

(ii) The applied moment is approximately proportional to the average in-plane curvature for $\bar{h} < 1$, despite geometric and material nonlinearity.

(iii) For a sufficiently large residual surface stress, the plate becomes unstable at a critical applied moment, as indicated by the green dash-dot line in Fig. 16.

(iv) The instability can be mitigated or even eliminated by increasing the surface tensile elasticity (red dotted line in Fig. 16).
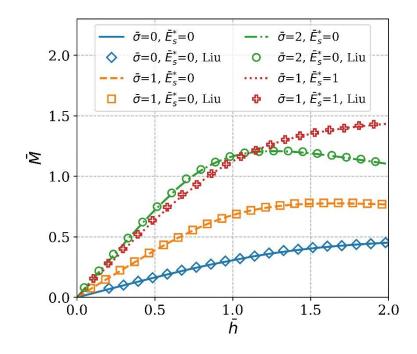
Fig. 16. Normalized applied moment versus normalized average in-plane curvature for different elasto-capillary and elasto-stiffening numbers. The symbols are Liu et al's results.

These conclusions might not be true when surface bending effect comes into play. Intuition suggest that surface bending moment $m_s^{11}$ is much more sensitive to curvature change compared to the surface stress $\sigma_s^{11}$; so for the same amount of bending, one should expect a drastic increase in applied moment if the surface bending is introduced.

First we consider the case $\sigma_0 = E_s^* = 0$ but $D_s \neq 0$. In Fig. 17(a) we plot the normalized applied moment versus the average in-plane curvature for different elasto-bending number $\bar{D}_s$. As Fig. 16 shows, the surface bending increases the applied moment dramatically. More interestingly, this bending process is stable, contrasting (iii) where the plate becomes unstable at some critical average in-plane curvature. Also, the linear relationship between applied moment and average in-plane curvature breaks down when $\bar{D}_s > 0.5$ (Fig. 17(a)), i.e., (ii) is no longer valid. To gain physical insight, in Fig. 17(b) and (c) we plot the distribution of circumferential $\bar{\sigma}_{\theta\theta}$ and radial true stress $\bar{\sigma}_{rr}$, respectively, at a given average in-plane curvature $\bar{h} = 1.0$. Fig. 17(b) shows that the surface bending makes $\bar{\sigma}_{\theta\theta}$ more compressive and more severe near the inner surface, which in return requires an additional applied bending for a fixed $\bar{h}$ (see Fig. 16a). Fig. 17(c) implies the inner part of the plate is radially stretched ($\bar{\sigma}_{rr} > 0$) and the outer is compressed ($\bar{\sigma}_{rr} < 0$) due to the surface bending, hence the thickness will vary during the plate bending process. To see this, we plot the variation of thickness against average in-plane curvature in Fig. 17(d) for different elasto-bending numbers. For the case of no surface stress effects ($\bar{D}_s = 0$), the plate thins as curvature increases; we name this the "thinning effect". This thinning effect is inhibited by surface bending. Indeed, for $\bar{D}_s = 1$, the thickness of the plate actually increases for small curvatures instead of decreasing, which provides an additional resistance to the plate bending.
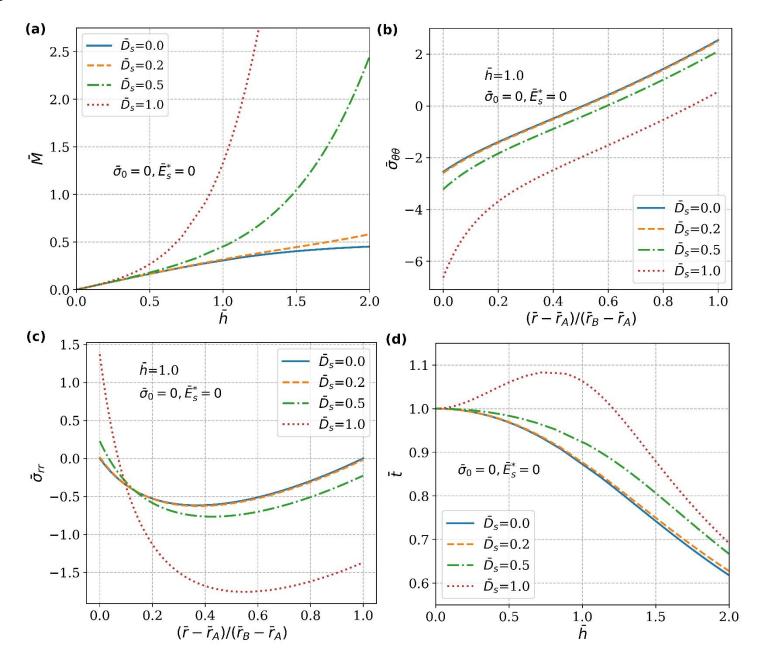
Fig. 17. (a) Normalized applied moment versus normalized average in-plane curvature for different elasto-bending numbers while $\sigma_0 = E_s^* = 0$; (b) distribution of circumferential $\bar{\sigma}_{\theta\theta}$ and (c) radial stress $\bar{\sigma}_{rr}$ at a given average in-plane curvature $\bar{h} = 1.0$; (d) normalized thickness versus normalized average in-plane curvature.

Finally, we consider the combined effects of surface bending and surface stress. As Fig. 18(a) shows, both surface stiffening and surface bending can stabilize bending. However, the increase in moment due to surface bending is much more significant than surface stiffening, especially at large curvatures. Fig. 18(b) plots the thickness change against the average in-plane curvature. Here the situation is reversed. Surface stiffening

makes the plate much thinner, while the surface bending stiffness makes the plate slightly thicker compared to the situation where $\bar{E}_s^* = \bar{D}_s = 0$.
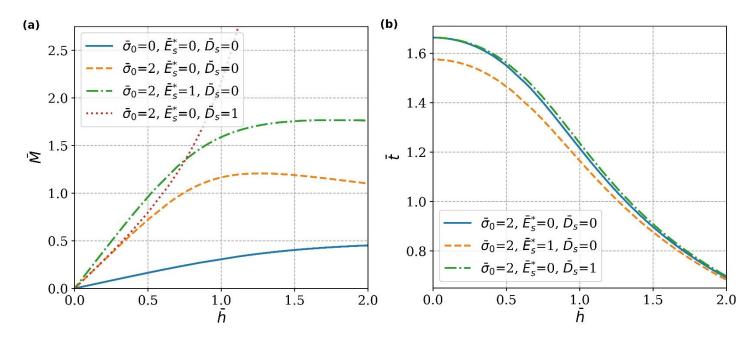


Fig. 18. (a) Normalized applied moment versus normalized average in-plane curvature considering combined effect of surface stiffening and surface bending with a fixed $\bar{\sigma}_0 = 2$; (b) normalized thickness versus normalized average in-plane curvature.

## 5. Conclusion

We review the general theory of surface-substrate interactions in which the surface bending, stretching and shearing are considered under the framework of large deformation. We then propose a Helmholtz free energy function for the surfaces that contain terms representative of the residual surface stress, surface tensile modulus and surface bending stiffness. We provide a detailed recipe to calculate the surface stress and surface bending and to formulate the in-plane equilibrium equations for 2D plane strain problems. We apply our plane strain theory to study how surface effects change the solution of two classical elasticity problems: the inflation of a cylindrical shell and the bending of a plate. The solution is obtained analytically in closed form. Previous studies [60,66] have shown that residual surface stress can increase the structural resistance to applied loads (for our two examples, the applied loads are inner pressure and applied moment, respectively). However, if the residual surface stress is sufficiently large, it can also cause structural instability (e.g., Fig. 10 and Fig. 16), especially in a force controlled experiment. Our results show that surface stiffening and surface bending can mitigate and even eliminate this instability. We also explore the thickness change of the bending plate and find an interesting result that in the presence of surface bending stiffness, the plate can be fattened during bending.

In our model, we assume that the cylindrical shell or plate is neo-Hookean solid. It has been well known that the neo-Hookean constitutive model works well for moderately large deformation (stretch ratio < 4). After this, the neo-Hookean model underestimates the stress due to strain hardening.[67]   It should be noted that most of the interesting phenomena occur before the neo-Hookean model breaks down. To study the behavior at very large strains,  our model can be easily extended by considering more realistic constitutive models for bulk elasticity.[67]   Another limitation in our model is that we don't take the structural buckling into consideration. However, the circumferential stress in our solution can be negative in the presence of residual surface stress (e.g., see Fig. 13(a)); in such case, the thin shell may buckle which potentially invalidates our above analysis. To determine whether a structure (e.g., an elastic ring) carrying both surface stress and bending moments buckles, more work is needed to explore the instability of a solid with those complex surface properties. Also, the solutions present above considered only simple geometries under specialized loading conditions.   In applications, numerical approach is necessary.  Our formulation can be readily incorporated in a finite element model to study large deformation problems with complex geometries. For example, by using the same surface stress and bending moment given by (42c,d), Lapinski et al.[39] has successfully implemented a new 3-node surface finite element for nonlinear, implicit, static, 2D plane strain finite element simulations that incorporated surface stretching and bending, and their simulations and experimental observations match quite well. In addition, one can relax the plane strain assumption by extending the FEM formulation to 3D.

The constitutive model we proposed (equation (20)) embodies several assumptions that invite experimental validation or verification.  Probably, in decreasing degree of confidence, we can state that surface stress at zero strain exists and is important, surface elasticity likely is present in several cases, and surface bending may or may not be important.  We believe that an important next step would be to investigate experimentally for typical soft solids if and when these contributions to the constitutive response are necessary to include.

# References

1  J. S. Rowlinson and B. Widom, *Molecular theory of capillarity*, Courier Corporation, 2013.

2  P.-G. de Gennes, F. Brochard-Wyart and D. Quéré, *Capillarity and wetting phenomena: drops, bubbles, pearls, waves*, Springer, New York, NY, 2010.

3  H.-J. Butt, K. Graf and M. Kappl, *Physics and chemistry of interfaces*, Wiley-VCH, Weinheim, 2003.

4  R. W. Style, A. Jagota, C.-Y. Hui and E. R. Dufresne, *Annual Review of Condensed Matter Physics*, 2017, **8**, 99–118.

5   J. Bico, É. Reyssat and B. Roman, *Annu. Rev. Fluid Mech.*, 2018, **50**, 629–659.

6   D. Paretkar, X. Xu, C.-Y. Hui and A. Jagota, *Soft Matter*, 2014, **10**, 4084–4090.

7   S. Mora, C. Maurini, T. Phou, J.-M. Fromental, B. Audoly and Y. Pomeau, *Phys. Rev. Lett.*, 2013, **111**, 114301.

8   A. Marchand, S. Das, J. H. Snoeijer and B. Andreotti, *Phys. Rev. Lett.*, 2012, **108**, 094301.

9   S. Mora, T. Phou, J.-M. Fromental, L. M. Pismen and Y. Pomeau, *Phys. Rev. Lett.*, 2010, **105**, 214301.

10  R. W. Style, R. Boltyanskiy, B. Allen, K. E. Jensen, H. P. Foote, J. S. Wettlaufer and E. R. Dufresne, *Nature Physics*, 2014, **11**, 82–87.

11  C.-Y. Hui, T. Liu and M.-E. Schwaab, *Extreme Mechanics Letters*, 2016, **6**, 31–36.

12  R. Thomson, T.-J. Chuang and I.-H. Lin, *Acta Metallurgica*, 1986, **34**, 1133–1143.

13  C. I. Kim, P. Schiavone and C.-Q. Ru, *Journal of Elasticity*, 2011, **104**, 397–420.

14  Z. Liu, K. E. Jensen, Q. Xu, R. W. Style, E. R. Dufresne, A. Jagota and C.-Y. Hui, *Soft Matter*, 2019, **15**, 2223–2231.

15  X. Xu, A. Jagota and C.-Y. Hui, *Soft Matter*, 2014, **10**, 4625–4632.

16  R. W. Style, C. Hyland, R. Boltyanskiy, J. S. Wettlaufer and E. R. Dufresne, *Nature Communications*, 2013, **4**, 2728.

17  Z. Cao, M. J. Stevens and A. V. Dobrynin, *Macromolecules*, 2014, **47**, 3203–3209.

18  J.-M. Y. Carrillo and A. V. Dobrynin, *Langmuir*, 2012, **28**, 10881–10890.

19  T. Salez, M. Benzaquen and É. Raphaël, *Soft Matter*, 2013, **9**, 10699.

20  B. Andreotti and J. H. Snoeijer, *Annu. Rev. Fluid Mech.*, 2020, **52**, 285–308.

21  A. Marchand, S. Das, J. H. Snoeijer and B. Andreotti, *Physical Review Letters*, 2012, **109**, 236101.

22  H. Wu, Z. Liu, A. Jagota and C.-Y. Hui, *Soft Matter*, 2018, **14**, 1847–1855.

23  E. R. Jerison, Y. Xu, L. A. Wilen and E. R. Dufresne, *Phys. Rev. Lett.*, 2011, **106**, 186103.

24  Z. Cao and A. V. Dobrynin, *Macromolecules*, 2015, **48**, 443–451.

25  R. W. Style, R. Boltyanskiy, Y. Che, J. S. Wettlaufer, L. A. Wilen and E. R. Dufresne, *Phys. Rev. Lett.*, 2013, **110**, 066103.

26  L. Limat, *The European Physical Journal E*, 2012, **35**, 134.

27  J. Dervaux and L. Limat, *Proceedings of the Royal Society A: Mathematical, Physical and Engineering Sciences*, 2015, **471**, 20140813.

28  J. H. Snoeijer, E. Rolley and B. Andreotti, *Phys. Rev. Lett.*, 2018, **121**, 068003.

29  J. Olives, *J. Phys.: Condens. Matter*, 2010, **22**, 085005.

30  T. Liu, Z. Liu, A. Jagota and C.-Y. Hui, *Journal of the Mechanics and Physics of Solids*, 2020, **138**, 103902.

31  Z. Liu, N. Bouklas and C.-Y. Hui, *Proceedings of the Royal Society A: Mathematical, Physical and Engineering Sciences*, 2020, **476**, 20190761.

32  K. E. Jensen, R. W. Style, Q. Xu and E. R. Dufresne, *Physical Review X*, 2017, **7**, 041031.

33  R. D. Schulman, M. Trejo, T. Salez, E. Raphaël and K. Dalnoki-Veress, *Nature Communications*, 2018, **9**, 982.

34  Helfrich W, *znc*, 2014, **28**, 693.

35  J. T. Jenkins, *Journal of Mathematical Biology*, 1977, **4**, 149–169.

36  H. Kusumaatmaja, Y. Li, R. Dimova and R. Lipowsky, *Physical Review Letters*, 2009, **103**, 238103.

37  C. M. Stafford, C. Harrison, K. L. Beers, A. Karim, E. J. Amis, M. R. VanLandingham, H.-C. Kim, W. Volksen, R. D. Miller and E. E. Simonyi, *Nature Materials*, 2004, **3**, 545–550.

38  P.-C. Lin, S. Vajpayee, A. Jagota, C.-Y. Hui and S. Yang, *Soft Matter*, 2008, **4**, 1830–1835.

39 N. Lapinski, Z. Liu, S. Yang, C.-Y. Hui and A. Jagota, *Soft Matter*, 2019, **15**, 3817–3827.

40 A. C. Eringen, *Journal of Mathematics and Mechanics*, 1966, **15**, 909–923.

41 W. Nowacki, *Theory of micropolar elasticity*, Springer, 1972.

42 D. J. Steigmann and R. W. Ogden, *Proceedings of the Royal Society of London. Series A: Mathematical, Physical and Engineering Sciences*, 1999, **455**, 437.

43 X. Gao, Z. Huang, J. Qu and D. Fang, *Journal of the Mechanics and Physics of Solids*, 2014, **66**, 59–77.

44 M. E. Gurtin and A. I. Murdoch, *Archive for Rational Mechanics and Analysis*, 1975, **57**, 291–323.

45 A. E. Green, P. M. Naghdi and W. L. Wainwright, *Archive for Rational Mechanics and Analysis*, 1965, **20**, 287–308.

46 C.-Y. Hui, Z. Liu and A. Jagota, *Extreme Mechanics Letters*, 2018, **23**, 9–16.

47 C.-Y. Hui, Z. Liu and A. Jagota, *Proceedings of the Royal Society A: Mathematical, Physical and Engineering Science*, 2018, **474**, 20170775.

48 C.-Y. Hui and A. Jagota, *Soft Matter*, 2015, **11**, 8960–8967.

49 R. Masurel, M. Roché, L. Limat, I. Ionescu and J. Dervaux, *Phys. Rev. Lett.*, 2019, **122**, 248004.

50 J. Dervaux, M. Roché and L. Limat, *Soft Matter*, 2020, **16**, 5157–5176.

51 A. Pandey, B. Andreotti, S. Karpitschka, G. J. van Zwieten, E. H. van Brummelen and J. H. Snoeijer, *arXiv:2003.09823 [cond-mat]*.

52 S. B. Hutchens, S. Fakhouri and A. J. Crosby, *Soft Matter*, 2016, **12**, 2557–2566.

53 R. Shuttleworth, *Proceedings of the Physical Society. Section A*, 1950, **63**, 444.

54 M. P. do Carmo, *Differential geometry of curves and surfaces*, Prentice-Hall, Englewood Cliffs, N.J, 1976.

55 Q. -s. Zheng, *Proceedings of the Royal Society of London. Series A: Mathematical and Physical Sciences*, 1993, **443**, 127–138.

56 A. N. Gent, P. B. Lindley and E. K. Rideal, *Proceedings of the Royal Society of London. Series A. Mathematical and Physical Sciences*, 1959, **249**, 195–205.

57 A. N. Gent and C. Wang, *Journal of Materials Science*, 1991, **26**, 3392–3395.

58 A. N. Gent and D. A. Tompkins, *Journal of Polymer Science Part A-2: Polymer Physics*, 1969, **7**, 1483–1487.

59 J. A. Zimberlin, N. Sanabria-DeLong, G. N. Tew and A. J. Crosby, *Soft Matter*, 2007, **3**, 763.

60 S. Kundu and A. J. Crosby, *Soft Matter*, 2009, **5**, 3963.

61 J. Dollhofer, A. Chiche, V. Muralidharan, C. Creton and C. Y. Hui, *International Journal of Solids and Structures*, 2004, **41**, 6111–6127.

62 M. L. Williams and R. A. Schapery, *Int J Fract*, 1965, **1**, 64–72.

63 J. Y. Kim, Z. Liu, B. M. Weon, T. Cohen, C.-Y. Hui, E. R. Dufresne and R. W. Style, *Sci Adv*, 2020, **6**, eaaz0418.

64 A. F. Bower, *Applied mechanics of solids*, CRC Press, Boca Raton, 2010.

65 A. E. Green and W. Zerna, *Theoretical elasticity*, Courier Corporation, 1992.

66 T. Liu, A. Jagota and C.-Y. Hui, *Soft Matter*, 2017, **13**, 386–393.

67 M. C. Boyce and E. M. Arruda, *Rubber Chemistry and Technology*, 2000, **73**, 504–523.